Application of the Stabilization Method to Temporary Anion States of CH3CN, CH3NC, CH3SCN, and CH3NCS in Density Functional Theory with Asymptotically Corrected Potentials

ARTICLE *in* THE JOURNAL OF PHYSICAL CHEMISTRY A · JANUARY 2011

Impact Factor: 2.69 · DOI: 10.1021/jp109466j · Source: PubMed

4 AUTHORS, INCLUDING:

Ki Wi Chen
Tunghai University
12 PUBLICATIONS **115** CITATIONS

Application of the Stabilization Method to Temporary Anion States of CH_3CN, CH_3NC, CH_3SCN, and CH_3NCS in Density Functional Theory with Asymptotically Corrected Potentials

Hsiu-Yao Cheng,* Chi-Wei Chen,† Jung-Tzu Chang,† and Chun-Chi Shih†

Department of Chemistry, Tunghai University, Taichung 40704, Taiwan

Received: October 2, 2010; Revised Manuscript Received: November 6, 2010

In this paper, density functional theory (DFT) with asymptotically corrected potentials is used to investigate CH_3CN, CH_3NC, CH_3SCN, and CH_3NCS molecules. For the energies of σ^* and π^* temporary anion states, the stabilized Koopmans' theorem (S-KT) using long-range correction functional and stabilized Koopmans-based (S-KB) approximation using local functional, are adopted. The stabilization procedure is accomplished by varying the exponents of appropriate diffuse functions. Results indicate that the calculations based on asymptotically corrected density functionals can yield better energy results of temporary anion states over conventional DFT methods.

1. Introduction

Cyanide, isocyanide, thiocyanate, and isothiocyanate have generated much interest due to their importance in organic synthesis, catalytic chemistry, organic conductors, nonlinear optics, photovoltaic devices, and medicinal applications.[1−6] For instance, the electron acceptors tetracyanoethene and tetracyanoquinodimethane are of interest in the area of molecular electronics. Ruthenium cyanide complexes are efficient charge-transfer sensitizers for photovoltaic cell. Many multicomponent reactions in chemistry are performed with isocyanides in drug discovery. Thiocyanate plays an important part in the biosynthesis of hypothiocyanite by lactoperoxidase. Isothiocyanates are important in the chemistry of heterocycles. Certain Isothiocyanates can inhibit the proliferation of cancer cells. These compounds resemble halides in many properties and are frequently classified as "pseudohalides". Nevertheless, these compounds differ from halides by the presence of π and unoccupied π^* molecular orbitals. These compounds also function as electron acceptors in many reactions. Hence, the determination of ionization potentials (IPs) and electron affinities (EAs) are imperative in understanding their bonding, catalytic properties, conductivity, and nonlinear optical activities.

In general, the IPs and EAs can be separately determined by means of photoelectron spectroscopy (PES)[7] and electron transmission spectroscopy (ETS)[8,9] experimentally. In the theoretical prediction of IPs and EAs, the Koopmans' theorem (KT)[10] approximation is usually adopted. The IPs and EAs in the KT approximation are associated with the negatives of the energies of the filled and unfilled orbitals, respectively. However, it neglects relaxation and correlation effects. Moreover, for species with negative EAs, the temporary anion (or resonance) is unstable with respect to electron detachment. Any variational calculations are likely to fail due to variational collapse to the neutral molecule plus a free electron for temporary anion states. Thus, the unfilled orbitals are prone to collapse onto approximations of continuum functions called orthogonalized discretized continuum (ODC)[11−13] solutions when large basis sets are used. Therefore, the energy calculations of temporary anion states using the KT approximation are unreliable.

When the DFT[14] method is used, the physical meaning of Kohn−Sham (KS) orbitals is unclear.[15,16] Most DFT potentials will not yield asymptotic behavior properly.[16−18] The errors for Koopmans' IPs/EAs in local, semilocal, and hybrid density functionals can be of several electronvolts. Various asymptotic correction (AC) schemes have been devised. In the long-range correction (LRC) scheme, the coulomb operator is usually divided into short-range (SR) and long-range (LR) parts by using the standard error function.[19−21] On the basis of the consideration of the integer discontinuity in the exact exchange−correlation potential, Tozer and co-workers have proposed an alternative Koopmans-based (KB) approximation using AC.[18]

The stabilization method proposed by Taylor and co-workers[22] can distinguish the temporary anion orbital solutions from the ODC solutions. The vertical attachment energies (AEs) are associated with the energies of the "stabilized" temporary anion states of the neutral molecules. By combining the stabilization method and consideration of LRC, we have applied the S-KT (i.e., the stabilization method coupled with KT) and S-KB (i.e., the stabilization method coupled with KB) in studying the π^* anion states of a series of molecules.[23] Results have indicated that the stabilization approach via DFT has yielded an improvement in predicting energies of temporary anion states over other approaches.

Temporary anion states associated with empty σ^* orbitals usually lie at higher energies and have lower potential barriers than those associated with π^* orbitals and thus give rise to shorter lifetime and broader shape resonances. The breadth of the structures usually makes it difficult to assign the resonance energy accurately. The σ^* and π^* temporary anion states of CH_3CN, CH_3NC, CH_3SCN, and CH_3NCS have been assigned previously.[12,24] Yet, some of the energies and characteristics of σ^*/π^* resonances remain uncertain. Furthermore, the stability of the σ^* anion states has not been systematically examined by using the DFT method. Hence, it is imperative to study the temporary anion states of these important compounds. In this study, the S-KT using LRC functional and the S-KB using local functional will be adopted. As to the filled molecular orbitals

* Corresponding author. E-mail: hycheng@thu.edu.tw. Telephone number: 011-886-4-23590248-102. Fax number: 011-886-4-23590426.

† E-mail: C.W.C., doremi1218@hotmail.com; J.T.C., tzu.cih@gmail.com; C.C.S. chunchi77726@hotmail.com.

10.1021/jp109466j
Published on Web 12/13/2010

(MOs), we will apply the KT and KB approximation to the IPs. Finally, the results will be compared with experimental values.

2. Computational Method

The IPs and EAs in the KT approximation can be written as $IP^{KT} \approx -\varepsilon_{OMO}$ and $EA^{KT} \approx -\varepsilon_{VMO}$, where ε_{OMO} and ε_{VMO} denote the occupied and virtual molecular orbital energies, respectively. The vertical attachment energy, i.e., the negative of EA, can then be represented as $AE^{KT} \approx \varepsilon_{VMO}$. The virtual orbital energy associated with temporary anion state is also known as AE. The AE obtained from KT approach will be denoted as ε_{VMO}.

When the alternative KB approximation is applied, the asymptotic correction of the Koopmans value is roughly $\varepsilon_{HOMO} + (E_{N-1} - E_N)$. Here, ε_{HOMO} is the highest-occupied molecular orbital (HOMO) energy determined from the DFT calculation using a local exchange−correlation functional on the neutral system. The E_N and E_{N-1} are the total electronic energies of the neutral and cation, respectively. By applying the correction term, we can write the IP and AE in the KB approximation as

$$IP^{KB} \approx -\varepsilon_{OMO} + [\varepsilon_{HOMO} + (E_{N-1} - E_N)] \quad (1)$$

and

$$AE^{KB} \approx \varepsilon_{VMO} + [\varepsilon_{HOMO} + (E_{N-1} - E_N)] \quad (2)$$

To distinguish the temporary anion state solutions from the virtual ODC ones, the stabilization method is employed. Two different Gaussian-type basis sets, designated as A and B, are used in our stabilization calculations. The convention of designation is explained as follows. For the C, N, and S atoms, the 6-31G(d)+$\alpha(sp)_1$ basis set A is formed by augmenting the 6-31G(d) basis set with the diffuse $(sp)_1$ function multiplied by a scale factor α (denoted by $\alpha(sp)_1$). The 6-31+G(d)+$\alpha(sp)_2$ basis set B is formed by augmenting the 6-31+G(d) basis set with the diffuse $\alpha(sp)_2$ function. The $(sp)_1$ and $(sp)_2$ functions have the exponents of 0.0562 and 0.0146 for the C atom, 0.0707 and 0.0213 for the N atom, and 0.0391 and 0.0135 for the S atom, respectively. The inclusion of additional diffuse d or f polarization functions on C, N, and S is found to be unimportant for the energies of resonance states.

As α increases, the ODC solutions may approach the temporary anion state orbital solutions in energy and lead to avoided crossing between the two types of solutions. The stabilization graphs are obtained by plotting the calculated energies (ε_{VMO}) as a function of the scale factor α. When the avoided crossing between temporary anion and ODC solutions occurs at their point of closest approach α_{ac}, the energy of the anion shape resonance is taken as the mean value of these two eigenvalues. More accurate energies can be obtained by means of analytical continuation procedure or density-of-state method.[25−27] However, the midpoint method adopted by Burrow et al. suffices our present purpose.[28]

In the present study, we adopt both (1) LRC functional via S-KT and (2) local functional via S-KB methods for the temporary anion states. For the LRC functional, we use ωB97XD, CAM-B3LYP, and LC-ωPBE functionals. The ωB97XD[19] functional includes LR HF exchange, a small fraction of SR HF exchange, a modified B97 SR exchange, B97 correlation density functional, and empirical dispersion corrections. The CAM-B3LYP[20] functional comprises 0.19 HF plus 0.81 Becke 1988 (B88) exchange interaction at SR, and 0.65 HF plus 0.35 B88 at LR. The LC-ωPBE[21] functional contains SR ωPBE exchange, LR HF exchange, and full range PBE correlation. The local functional chosen is the PBEPBE[29] which utilizes pure generalized gradient approximation (GGA) functional. As to the HF method, it is also employed.

All calculations are performed using the Gaussian 09 program.[30] Geometric optimizations of all molecules are carried out at the B3LYP/6-31+G(d) level. The geometries of CH_3CN and CH_3NC are optimized under C_{3v}, and the geometries of CH_3SCN and CH_3NCS are optimized under C_s symmetry constraints. The optimized geometries are confirmed to be real minima via frequency analysis. However, in the case of CH_3NCS, the C_s geometric optimization always converges with one imaginary frequency, which is associated with the internal rotation of the methyl group. Although the C_s geometry is not the global minimum, its calculated orbital energies differ only slightly (<0.1 eV) from that of the C_1 geometry of the global minimum. Both CH_3SCN and CH_3NCS isomers are bent. The optimized bond angles of CH_3-S-CN and CH_3-NCS are 99.8 and 154.3°, respectively. The CN bond distances in CH_3CN and CH_3SCN are shorter (0.02 Å) than those of CH_3NC and CH_3NCS, respectively. As for energies, the total energies of CH_3CN and CH_3NCS are lower than those of CH_3NC and CH_3SCN, respectively.

3. Results and Discussion

The calculated IPs for CH_3CN and CH_3NC are tabulated along with the experimental values in Table 1. Here, we perform KT calculations using ωB97XD, LC-ωPBE, CAM-B3LYP, and HF ($KT^{\omega B97XD}$, $KT^{LC\text{-}\omega PBE}$, $KT^{CAM\text{-}B3LYP}$, and KT^{HF}), and KB calculations using PBEPBE (KB^{PBEPBE}) methods on the filled orbitals for these pseudohalides. In the table, the KT calculations using the PBEPBE and B3LYP (KT^{PBEPBE} and KT^{B3LYP}) methods are also employed for comparison. To compare with experimental results, corrected IPs are also included in the tables. The corrected values are obtained by shifting the amount from the calculated IP values to bring the highest cation states of CH_3CN and CH_3NC into agreement with the experimental values. As can be seen from Table 1, the increasing order of IPs of filled MOs are $2e < 7a_1 < 1e < 6a_1$ for CH_3CN and $7a_1 < 2e < 1e < 6a_1$ for CH_3NC.

In Table 1, when using the AC scheme of DFT, the mean errors of IPs for $KT^{\omega B97XD}$, $KT^{CAM\text{-}B3LYP}$, $KT^{LC\text{-}\omega PBE}$, and KB^{PBEPBE} methods are 0.63−0.99, 1.11−1.53, 0.11−0.39, and 0.16−0.52 eV, respectively. For the conventional DFT functionals, the errors of IPs for KT^{PBEPBE} and KT^{B3LYP} methods are 4.44−4.73 and 2.72−3.34 eV, respectively. They are much larger than those of the aforementioned AC approaches. As indicated in Table 1, the KT^{HF} method (∼1 eV mean error for IPs) also provides better results than those of the KT^{PBEPBE} and KT^{B3LYP} methods. It is possibly due to the fact that the neglect of correlation effect in HF method tends to cancel the relaxation error for IPs. As to the relative IPs (ΔIPs) between the HOMOs and the other cation states, Table 1 demonstrates that the DFT approaches generate more accurate ΔIPs than those of the HF method. The average errors for ΔIPs as compared to experimental values for AC DFT and HF methods are about 0.2 and 0.9 eV, respectively.

We then examine the characteristics of MOs for CH_3CN and CH_3NC. The correlation diagrams of the frontier MOs of CH_3CN and CH_3NC are illustrated in Figure 1. Our symmetry in the labeling of the orbital is based on the z axis being along the principal axis. In Figure 1, the ordering of MOs for CH_3 and CN/NC are estimated using the CH_3CN/CH_3NC structures

TABLE 1: Calculated and Corrected[a] IPs (eV) for CH_3CN and CH_3NC

		CH_3CN				CH_3NC			
method	basis set	e	a_1	e	a_1	a_1	e	e	a_1
$KT^{\omega B97XD}$	6-31G(d)	11.13	12.14	14.99	16.44	10.40	11.30	15.30	17.46
		(12.22	13.24	16.08	17.53)	(11.21	12.11	16.11	18.27)
	6-31+G(d)	11.37	12.42	15.14	16.62	10.79	11.60	15.49	17.68
		(12.22	13.27	15.99	17.47)	(11.21	12.02	15.91	18.10)
$KT^{CAM\text{-}B3LYP}$	6-31G(d)	10.57	11.60	14.47	15.89	9.84	10.75	14.79	16.93
		(12.22	13.25	16.11	17.54)	(11.21	12.12	16.16	18.30)
	6-31+G(d)	10.88	11.94	14.66	16.13	10.30	11.10	15.02	17.19
		(12.22	13.28	16.01	17.47)	(11.21	12.01	15.93	18.10)
$KT^{LC\text{-}\omega PBE}$	6-31G(d)	12.13	13.09	16.06	17.45	11.41	12.29	16.42	18.48
		(12.22	13.17	16.15	17.54)	(11.21	12.09	16.22	18.28)
	6-31+G(d)	12.36	13.35	16.21	17.63	11.77	12.57	16.60	18.69
		(12.22	13.21	16.07	17.49)	(11.21	12.01	16.04	18.13)
KB^{PBEPBE}	6-31G(d)	11.96	12.36	15.48	16.8	10.95	12.29	15.95	17.98
		(12.22	12.62	15.74	17.06)	(11.21	12.55	16.21	18.24)
	6-31+G(d)	12.11	12.56	15.52	16.87	11.19	12.39	15.92	17.99
		(12.22	12.67	15.63	16.98)	(11.21	12.41	15.94	18.01)
KT^{PBEPBE}	6-31G(d)	7.75	8.16	11.27	12.58	6.60	7.94	11.60	13.63
		(12.22	12.63	15.74	17.05)	(11.21	12.55	16.21	18.24)
	6-31+G(d)	8.07	8.52	11.48	12.82	7.11	8.31	11.84	13.91
		(12.22	12.67	15.64	16.97)	(11.21	12.41	15.94	18.01)
KT^{B3LYP}	6-31G(d)	8.87	9.74	12.64	14.05	8.02	9.06	12.96	15.09
		(12.22	13.09	15.99	17.39)	(11.21	12.25	16.15	18.28)
	6-31+G(d)	9.18	10.08	12.84	14.28	8.49	9.42	13.18	15.36
		(12.22	13.12	15.88	17.32)	(11.21	12.14	15.90	18.08)
KT^{HF}	6-31G(d)	12.40	14.97	17.04	18.97	12.61	12.67	17.33	20.03
		(12.22	14.79	16.86	18.79)	(11.21	11.27	15.93	18.63)
	6-31+G(d)	12.57	15.15	17.14	19.10	12.89	12.84	17.46	20.16
		(12.22	14.80	16.79	18.75)	(11.21	11.16	15.78	18.48)
expt[b]		12.22	13.14	15.8,16.3	17.5	11.21	12.35	16.2,16.8	18.3

[a] The corrected values (shown in parentheses) are obtained by shifting the amount needed to bring the calculated IPs into agreement with experimental values for the HOMOs. [b] The experimental IPs for CH_3CN and CH_3NC are taken from ref 32.

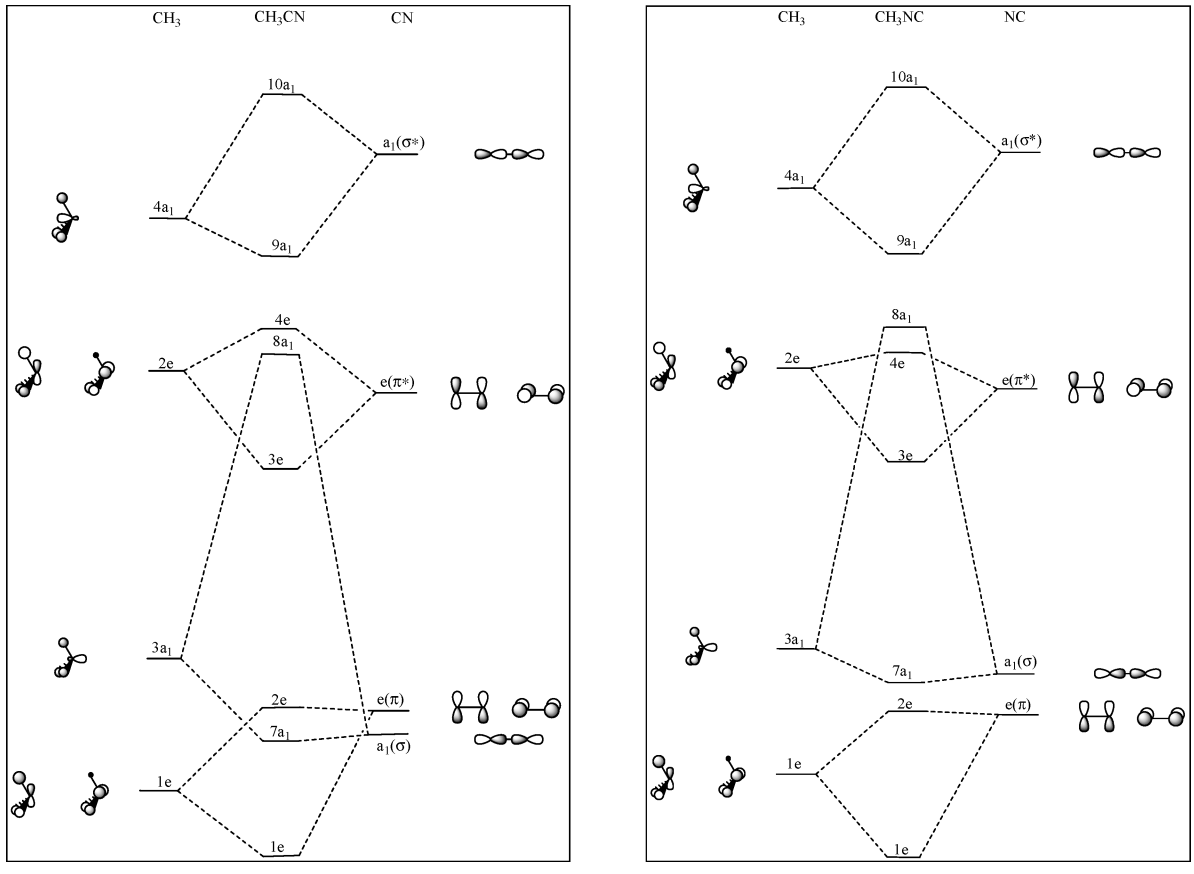

Figure 1. Correlation diagram of the frontier MOs for CH_3CN and CH_3NC.

TABLE 2: Calculated and Corrected[a] IPs (eV) for CH_3SCN and CH_3NCS[b]

		KT^{wB97XD}		$KT^{CAM\text{-}B3LYP}$		$KT^{Lc\text{-}wPBE}$		KB^{PBEPBE}		KT^{HF}		
		A_0	B_0	A_0	B_0	A_0	B_0	A_0	B_0	A_0	B_0	expt[c]
CH_3SCN	a″	9.38	9.54	8.80	9.01	10.22	10.37	9.70	9.83	10.40	10.51	10.25
		(10.25)	(10.25)	(10.25)	(10.25)	(10.25)	(10.25)	(10.25)	(10.25)	(10.25)	(10.25)	
	a′	11.22	11.41	10.65	10.90	12.17	12.35	11.41	11.58	12.30	12.43	12.10
		(12.09)	(12.12)	(12.10)	(12.14)	(12.20)	(12.23)	(11.96)	(12.00)	(12.15)	(12.17)	
	a′	12.28	12.51	11.73	12.02	13.25	13.47	11.80	12.03	13.98(a″)	14.11(a″)	12.88
		(13.15)	(13.22)	(13.18)	(13.26)	(13.28)	(13.35)	(12.35)	(12.45)	(13.83)	(13.85)	
	a″	12.48	12.67	11.92	12.17	13.61	13.80	12.31	12.48	14.43(a′)	14.55(a′)	13.1
		(13.35)	(13.38)	(13.37)	(13.41)	(13.64)	(13.68)	(12.86)	(12.90)	(14.28)	(14.29)	
	a′	13.25	13.41	12.68	12.88	14.25	14.40	13.17	13.28	15.29	15.43	13.75
		(14.12)	(14.12)	(14.13)	(14.12)	(14.28)	(14.28)	(13.72)	(13.70)	(15.14)	(15.17)	
	a′	14.58	14.71	14.04	14.21	15.60	15.72	14.42	14.51	16.56	16.65	15.1
		(15.45)	(15.42)	(15.49)	(15.45)	(15.63)	(15.60)	(14.97)	(14.93)	(16.41)	(16.39)	
	a″	14.96	15.08	14.44	14.60	16.04	16.15	14.67	14.75	17.09	17.16	15.9
		(15.83)	(15.79)	(15.89)	(15.84)	(16.07)	(16.03)	(15.22)	(15.17)	(16.94)	(16.90)	
CH_3NCS	a″	8.70	8.83	8.10	8.27	9.46	9.57	9.09	9.19	9.50	9.59	9.42
		(9.42)	(9.42)	(9.42)	(9.42)	(9.42)	(9.42)	(9.42)	(9.42)	(9.42)	(9.42)	
	a′	8.83	8.96	8.23	8.40	9.58	9.70	9.23	9.33	9.63	9.73	9.42
		(9.55)	(9.55)	(9.55)	(9.55)	(9.54)	(9.55)	(9.56)	(9.56)	(9.55)	(9.56)	
	a′	12.64	12.75	12.09	12.24	13.74	13.84	12.36	12.44	14.31	14.38	12.60
		(13.36)	(13.34)	(13.41)	(13.39)	(13.70)	(13.69)	(12.69)	(12.67)	(14.23)	(14.21)	
	a″	12.65	12.77	12.11	12.26	13.77	13.87	12.39	12.47	14.31	14.38	12.60
		(13.37)	(13.36)	(13.43)	(13.41)	(13.73)	(13.72)	(12.72)	(12.70)	(14.23)	(14.21)	
	a′	14.05	14.19	13.48	13.66	14.97	15.09	13.81	13.90	15.95	16.06	14.58
		(14.77)	(14.78)	(14.80)	(14.81)	(14.93)	(14.94)	(14.14)	(14.13)	(15.87)	(15.89)	
	a″	15.46	15.54	14.95	15.07	16.65	16.72	14.97	15.01	17.71	17.76	15.9
		(16.18)	(16.13)	(16.27)	(16.22)	(16.61)	(16.57)	(15.30)	(15.24)	(17.63)	(17.59)	
	a′	15.47	15.56	14.97	15.09	16.66	16.73	14.99	15.03	17.75	17.80	15.9
		(16.19)	(16.15)	(16.29)	(16.24)	(16.62)	(16.58)	(15.32)	(15.26)	(17.67)	(17.63)	

[a] The corrected values (shown in parentheses) are obtained by shifting the amount needed to bring the calculated IPs into agreement with experimental values for the HOMOs. [b] A_0 and B_0 denote the 6-31G(d) and 6-31+G(d) basis sets, respectively. [c] The IPs are taken from ref 33.

by setting up the other atoms as ghost atoms[30] via KT. The relevant MOs of CH_3CN and CH_3NC molecules may be derived from the a_1 and e orbitals of the CH_3 group and the CN/NC group. The C atom in CH_3 is designated as C_I. In the C_{3v} point group, the 2p orbitals of C_I yield a_1 ($2p_z$) and e ($2p_{x,y}$) orbitals, and the three 1s orbitals of H atoms yield a_1 and e orbitals. For the CH_3 group, the $3a_1(\sigma)$ and $4a_1(\sigma^*)$ result from bonding and antibonding a_1 C_I ($2p_z$) with that of H (1s). The 1e (pseudo-π) and 2e (pseudo-π^*) orbitals of CH_3 result from bonding and antibonding of e orbitals of C_I ($2p_{x,y}$) with those of H (1s). As for the CN/NC group, the σ/σ^* orbitals are of a_1 symmetries and π/π^* orbitals are of e symmetries. Both CH_3CN and CH_3NC molecules have seven a_1 and two e occupied orbitals. For both molecules, the 2e orbitals correspond to π-antibonding interaction between π_{C-N}/π_{N-C} and pseudo-π_{CH_3}. The 1e orbitals correspond to π-bonding interaction between π_{C-N}/π_{N-C} and pseudo-π_{CH_3}. The $7a_1$ results from the mixing of $3a_1$ of CH_3 with σ_{C-N}. The $6a_1$ results from the mixing of 2s orbitals of all atoms.

Table 2 lists the calculated IPs for CH_3SCN and CH_3NCS. For CH_3SCN, the increasing orders of IPs of filled MOs are $4a'' < 15a' < 14a' < 3a'' < 13a' < 12a' < 2a''$. As for CH_3NCS, the increasing orders of IPs for filled MOs are $4a'' \approx 15a' < 14a' \approx 3a'' < 13a' < 2a'' \approx 12a'$ for all AC DFT methods. According to Table 2, the average errors for IPs are around 0.50, 1.00, 0.53, and 0.60 eV for the $KT^{\omega B97XD}$, $KT^{CAM\text{-}B3LYP}$, $KT^{LC\text{-}\omega PBE}$, and KB^{PBEPBE} methods, respectively. If the HF method is used, the orders of 3a″ and 14a′ orbitals for CH_3SCN are not conformable with those of DFT approaches. The HF calculations lead to ~1.2 eV average errors for IPs. As to the ΔIPs, the HF generates larger errors of ΔIPs (~1.0−1.4 eV) than the DFT methods (~0.2−0.7 eV). To sum up, the AC DFT approaches generally yield better ΔIPs as compared to the HF method. One possible reason for this is because the DFT approach contains exchange−correlation potential.[15]

The correlation diagrams of the frontier MOs of CH_3SCN and CH_3NCS molecules are illustrated in Figure 2. The relevant MOs of CH_3SCN/CH_3NCS may be derived from a′ and a″ orbitals of CH_3 and SCN/NCS constituents. In the C_s point group, the in-plane π orbitals, denoted as $\pi_{||}$, are of a′ symmetry and the out-of-plane π orbitals, denoted as $\pi_{\perp}$, are of a″ symmetry. For the CH_3 group, the 1a″ and 3a′ orbitals are pseudo-$\pi_{\perp}$ and pseudo-$\pi_{||}$, and the 5a′ and 2a″ orbitals are pseudo-$\pi^*_{||}$ and pseudo-$\pi^*_{\perp}$, respectively. The 4a′ and 6a′ are the σ and σ^* orbitals. For the SCN/NCS groups, the 2a″ ($\pi_{\perp+}$) and 3a″ ($\pi_{\perp-}$) orbitals result from the π bonding and antibonding interactions between CN/NC ($\pi_{\perp}$) and a″ of S (3p). The 4a″ ($\pi^*_{\perp}$) orbital is derived from the mixing of CN/NC ($\pi^*_{\perp}$) with a″ of S (3p). The 10a′ ($\pi_{||+}$) and 12a′ ($\pi_{||-}$) orbitals result from the π bonding and antibonding interactions between CN/NC ($\pi_{||}$) and a′ of S (3p). The 13a′ ($\pi^*_{||}$) orbital results from the mixing of CN/NC ($\pi^*_{||}$) with a′ of S (3p) orbitals. The 11a′ (σ) corresponds to the bonding interactions between CN/NC (σ) and a′ of S (3p). The 14a′ and 15a′ (σ^*) orbitals result from the mixing of CN/NC (σ^*) with a' of S (3p).

Both CH_3SCN and CH_3NCS molecules have fifteen a'' and four a″ occupied MOs. For the CH_3SCN molecule, the 4a″ orbital is HOMOs. The 4a″ orbital is essentially from the SCN a″($\pi_{\perp-}$) orbital. The 15a′ orbital corresponds to the bonding interaction between SCN a′($\pi_{||-}$) and 4a′(σ) of CH_3. The 14a′ orbital is mainly from the σ localized on the nitrogen. The 3a″ orbital results from the π-antibonding interaction between SCN a″($\pi_{\perp+}$) and pseudo-$\pi_{\perp,CH_3}$. The 13a′ orbital results from the π-antibonding interaction between SCN a′($\pi_{||+}$) and pseudo-$\pi_{||,CH_3}$. The 12a′ orbital corresponds to π-bonding interaction between CH_3 pseudo-$\pi_{||}$ and SCN a′($\pi_{||+}$). The 2a″ orbital

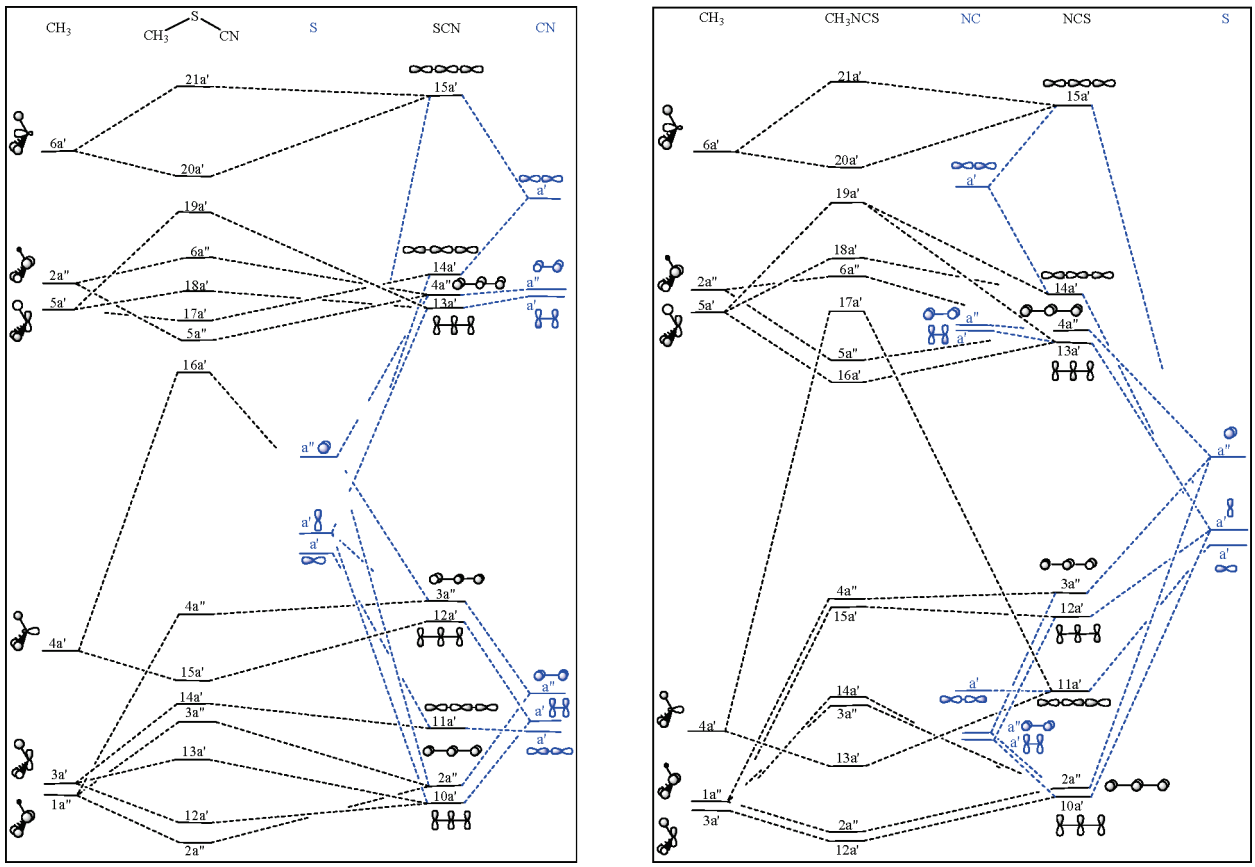

Figure 2. Correlation diagram of the frontier MOs for CH_3SCN and CH_3NCS.

corresponds to the bonding interaction between the CH_3 pseudo-$\pi_\perp$ orbital and SCN a″($\pi_{\perp+}$). As for the CH_3NCS molecule, the HOMO 4a″ is almost degenerate with 15a′. The 4a″ and 15a′ orbitals are essentially the NCS a″($\pi_{\perp-}$) and a′($\pi_{\parallel-}$) orbitals, respectively. The 14a′ and 3a″ orbitals are almost degenerate. The 14a′ orbital results from the π-antibonding interaction between NCS a′($\pi_{\parallel+}$) and pseudo-$\pi_{\parallel,CH_3}$ orbitals. The 3a″ results from the π-antibonding interaction between NCS a″($\pi_{\perp+}$) and pseudo-$\pi_{\perp,CH_3}$. The 13a′ orbital is mainly from the σ localized on the sulfur. The 2a″ and 12a′ orbitals are close in energy. The 2a″ orbital corresponds to the π-bonding interaction between CH_3 pseudo-$\pi_\perp$ and NCS a″($\pi_{\perp+}$) orbitals, and the 12a′ orbital results from the π-bonding interaction between CH_3 pseudo-$\pi_\parallel$ and NCS a′ ($\pi_{\parallel+}$) orbitals.

For the temporary anion shape resonance, we perform S-KT calculations on the unfilled orbitals to distinguish them from the ODC solutions for α between 0.0 and 3.0 via ωB97XD, CAM-B3LYP, LC-ωPBE, and HF (S-KT$^{\omega B97XD}$, S-KT$^{CAM\text{-}B3LYP}$, S-KT$^{LC\text{-}\omega PBE}$, and S-KT^{HF}) methods, and the S-KB calculations via PBEPBE (S-KB^{PBEPBE}). Figure 3 shows the energies of the discretized continuum (DC)[11−13] solutions as a function of scale factor α for the virtual orbitals of CH_3CN, CH_3NC, CH_3SCN, and CH_3NCS using the basis set A located at the appropriate nuclear positions. The energies of the DC solutions are obtained by solving the Kohn−Sham equation for a single electron in the absence of any potential.[11] As can be seen in Figure 3, all DC solutions increase with increasing α.

We will first present the results for CH_3CN and CH_3NC molecules. The stabilization graphs of the energies as a function of α for the e and a_1 virtual orbitals of CH_3CN and CH_3NC using basis set A for the S-KT$^{\omega B97XD}$ calculations are shown in Figure 4a,b, respectively. There are two types of energies for virtual orbital solutions in the stabilization calculations. One is the unfilled orbital solution and the other the ODC virtual orbital solution. The unfilled orbital solution and the ODC solutions are readily distinguished by examining how their energies vary with α and/or by comparing their solutions with the free electron DC solutions. Based also on examining the nature of virtual orbitals for the e virtual orbitals of CH_3CN as shown in Figure 4a, the fourth solution for $\alpha < 0.2$, the third solution for $0.2 < \alpha < 0.6$, the second solution for $0.6 < \alpha < 0.8$, and the first solution for $\alpha > 0.8$ are mainly from the 3e π^* orbital solution. The avoided crossings resulting from the couplings between the first and second solutions, the second and third solutions, and the third and fourth solutions are located at $\alpha_{ac}(1,2) = 0.8$, $\alpha_{ac}(2,3) = 0.6$, and $\alpha_{ac}(3,4) = 0.2$, respectively. The energies of the π^* orbital can be extracted from each avoided crossing region. The energies of 3e orbitals obtained are 2.83, 2.99, and 2.67 eV at $\alpha_{ac}(1,2)$, $\alpha_{ac}(2,3)$, and $\alpha_{ac}(3,4)$, respectively. The average value from each set of energy values will be defined as the energy of the 3e orbital. Thus, the energy of the 3e orbital is 2.83 eV. Similarly, the fifth solution for $\alpha < 0.8$, the fourth solution for $0.8 < \alpha < 1.4$, the third solution for $1.4 < \alpha < 2.0$, and the second solution for $\alpha > 2.0$ are mainly from the 4e π^* orbital solution. The energies of 4e orbitals obtained from the three avoided crossings are 6.66, 6.93, and 7.21 eV at $\alpha_{ac}(2,3) = 2.0$, $\alpha_{ac}(3,4) = 1.4$, and $\alpha_{ac}(4,5) = 0.8$, respectively. Accordingly, the energy of the 4e orbital is 6.93 eV. As for the a_1 virtual orbitals, the energies of the $8a_1$ obtained from the avoided crossings are 6.38 eV at $\alpha_{ac}(2,3) = 2.6$, 6.21 eV at $\alpha_{ac}(4,5) = 0.8$, and 7.15 eV at $\alpha_{ac}(7,8) = 0.8$. The energies of the $9a_1$ obtained from the avoided crossings are 11.48 eV at $\alpha_{ac}(6,7) = 1.4$ and 10.85 eV at $\alpha_{ac}(7,8) = 1.2$. Hence, the energies of the $8a_1$ and $9a_1$ orbitals are 6.58 and 11.17 eV,

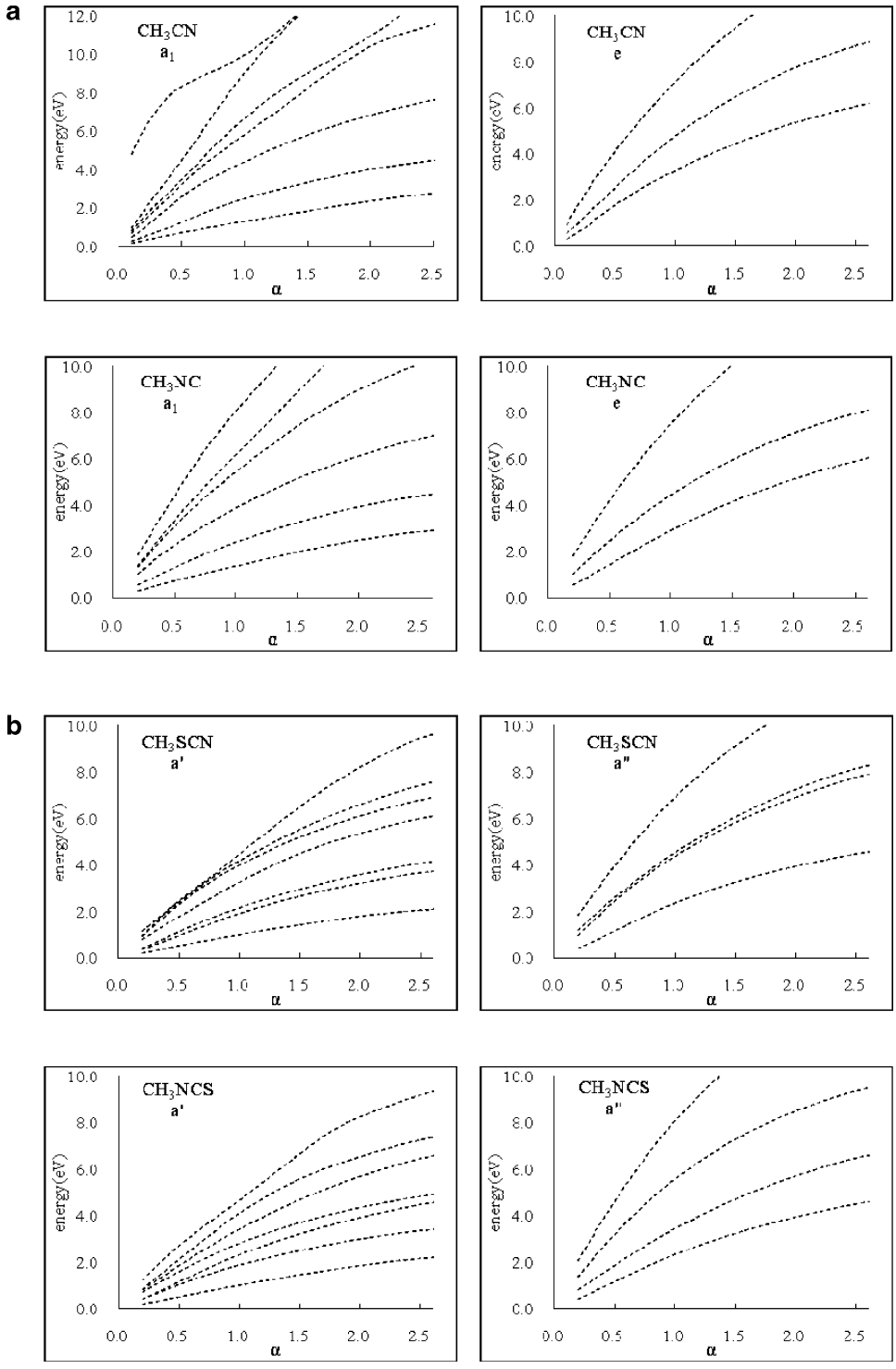

Figure 3. Energies of virtual orbitals of (a) CH_3CN and CH_3NC and (b) CH_3SCN and CH_3NCS as a function of the scaling factor α for a free electron in the absence of potentials.

respectively. According to our analysis of the CH_3CN molecule, as can be seen in Figure 1, the 3e orbitals essentially result from the π-bonding interaction between pseudo-$\pi^*_{CH_3}$ and π^*_{C-N}. The 4e orbitals result from the π-antibonding interaction between pseudo-$\pi^*_{CH_3}$ and π^*_{C-N}. The $8a_1$ orbital results from the antibonding interaction between $3a_1(\sigma)$ of CH_3 and σ_{C-N}. The $9a_1$ orbital results from the bonding interaction between $\sigma^*_{CH_3}$ and σ^*_{C-N}.

Next for CH_3NC, the energy of the 3e orbital obtained from the avoided crossing is 3.08 eV at $\alpha_{ac}(3,4) = 0.3$. The energies of 4e orbitals obtained from the avoided crossings are 6.30 eV at $\alpha_{ac}(2,3) = 2.0$, 6.92 eV at $\alpha_{ac}(3,4) = 1.4$, and 6.89 eV at $\alpha_{ac}(4,5) = 0.8$. Thus, the energy of the 4e orbital is 6.70 eV. For a_1 states, the energies of the $8a_1$ obtained are 7.12 eV at $\alpha_{ac}(5,6) = 0.8$ and 6.42 eV at $\alpha_{ac}(6,7) = 0.5$. Thus, the energy of the $8a_1$ orbital is 6.77 eV. The energy of the $9a_1$ obtained from the avoided crossing is 10.80 eV at $\alpha_{ac}(6,7) = 1.4$. According to our analysis for CH_3NC molecule, the 3e orbitals result from the π-bonding interaction between pseudo-$\pi^*_{CH_3}$ and π^*_{N-C}. The 4e orbitals result from the π-antibonding interaction between pseudo-$\pi^*_{CH_3}$ and π^*_{N-C}. The $8a_1$ orbital results from the antibonding interaction

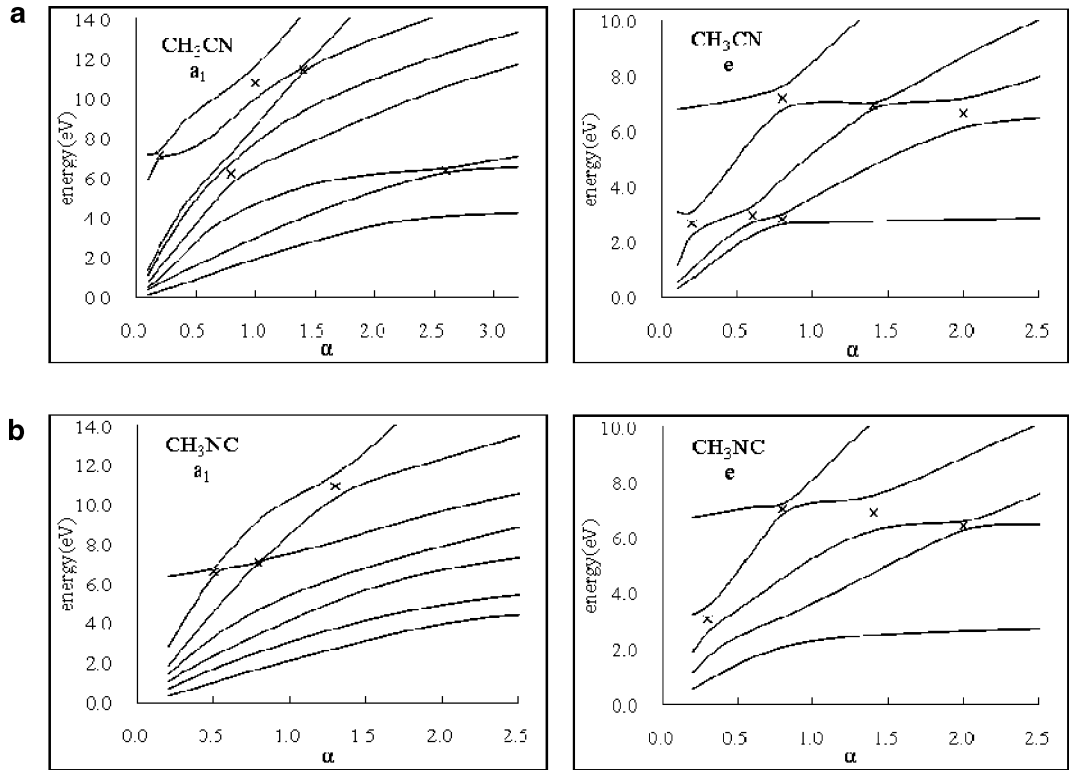

Figure 4. Stabilization graphs for CH_3CN and CH_3NC via the S-KT$^{\omega B97XD}$ method. Energies of a_1 and e virtual orbitals of (a) CH_3CN and (b) CH_3NC as a function of α. The location of α_{ac} is marked with x.

between CH_3 $3a_1(\sigma)$ and σ_{N-C}. The $9a_1$ orbital is derived from the mixing of $\sigma^*_{CH_3}$ with σ^*_{C-N}.

Table 3 illustrates the results of AEs using the stabilization methods for CH_3CN and CH_3NC along with their experimental values. The results of AEs using KT^{PBEPBE} and KT^{B3LYP} methods are also included for comparison. In the table, the AEs obtained via the S-KT$^{LC\text{-}\omega PBE}$ and S-KT^{PBEPBE} methods are larger than those obtained from the S-KT$^{\omega B97XD}$ and S-KT$^{CAM\text{-}B3LYP}$ methods. The S-KT$^{\omega B97XD}$ and S-KT$^{CAM\text{-}B3LYP}$ methods might give AEs less than experimental values. Possible reasons for these are that the KT approximation neglects relaxation and correlation effects and the inexact nature of the exchange−correlation functionals. The AEs obtained from the S-KT^{HF} method are larger than those obtained from all the DFT methods. As for relative AEs, the results from the S-KT^{HF} method are in excellent agreement with experiment. The DFT methods generate less accurate relative AEs than those of the HF method. Possible reasons for the discrepancy are due to the different considerations of exchange−correlation potential, self-interaction effect, and Coulomb contributions at large electron−molecule distance among these methods.[34,35] As can be seen from Table 3, the increasing order of AEs of unfilled MOs are $3e < 8a_1 < 4e < 9a_1$ for CH_3CN and $3e < 4e < 8a_1 < 9a_1$ for CH_3NC in all stabilization calculations. Nevertheless, the orders of AEs using the KT^{PBEPBE} and KT^{B3LYP} methods without the stabilization procedure are not definitive. In addition, the KT methods generally yield worse AEs than those of the S-KT/S-KB calculations.

According to our stabilization calculations for the assignments of the shape resonance observed in ET spectrum on CH_3CN molecule, the 2.82 eV feature in the ET spectrum is ascribed to electron capture into the empty 3e orbitals. The resonances at 5.7 and 6.8 eV are associated with the capture into $8a_1$ and 4e orbitals. Similarly for CH_3NC, the electron capture into 3e orbitals corresponds to the resonance at 2.81 eV. The resonances at 5.5 and 6.7 eV can be ascribed to the electron capture into 4e and $8a_1$ orbitals. For both molecules, the electron addition to the $9a_1$ orbital is not reported in the ET spectrum. One possible reason for this is that the $9a_1$ orbital lies at a relatively high energy and with broad width. Consequently, it makes the detection via ETS difficult. Notice that our assignments of the 4e π^* for both molecules differ from those of the previous studies that were based on energy loss measurements of C−H-containing species.[24]

Now for CH_3SCN and CH_3NCS, the stabilization graphs of the energies as a function of α for the a′ and a″ virtual orbitals of CH_3SCN and CH_3NCS using basis set A for the S-KT$^{\omega B97XD}$ calculations are shown in Figure 5a,b, respectively. For CH_3SCN in Figure 5a, the 5a″ orbital solution interacts with three ODC solutions. The obtained energies of the 5a″ orbital are 2.67 eV at $\alpha_{ac}(1,2) = 1.0$, 2.77 eV at $\alpha_{ac}(2,3) = 0.6$, and 2.65 eV at $\alpha_{ac}(3,4) = 0.4$. The 6a″ orbital solution interacts with four ODC solutions. The obtained energies of the 6a″ orbital are 5.99 eV at $\alpha_{ac}(2,3) = 2.6$, 6.10 eV at $\alpha_{ac}(3,4) = 1.6$, 6.62 eV at $\alpha_{ac}(4,5) = 1.4$, and 6.77 eV at $\alpha_{ac}(5,6) = 0.75$. Thus, the energies of the 5a″ and 6a″ orbitals are 2.70 and 6.37 eV, respectively.

For the a′ virtual orbitals, the energy obtained for the 16a′ is 1.32 eV at $\alpha_{ac}(3,4) = 0.5$. The energies obtained for the 17a′ orbital are 3.17 eV at $\alpha_{ac}(3,4) = 1.7$ and 2.89 eV at $\alpha_{ac}(4,5) = 1.1$. The energies obtained for the 18a′ orbital are 4.36 eV at $\alpha_{ac}(6,7) = 1.3$, 3.93 eV at $\alpha_{ac}(7,8) = 0.9$, 3.94 eV at $\alpha_{ac}(8,9) = 0.8$, 3.37 eV at $\alpha_{ac}(9,10) = 0.5$, and 4.21 eV at $\alpha_{ac}(13,14) = 0.4$. The energies obtained for the 19a′ orbital are 9.31 eV at $\alpha_{ac}(13,14) = 1.4$, 8.31 eV at $\alpha_{ac}(14,15) = 1.0$, and 6.89 eV at $\alpha_{ac}(15,16) = 0.5$. The energies obtained for 20a′ orbital are 11.91 eV at $\alpha_{ac}(14,15) = 1.8$ and 10.75 eV at $\alpha_{ac}(16,17) = 0.9$. According to our analysis, the avoided crossings at $\alpha_{ac}(10,11) = 0.9$ and $\alpha_{ac}(12,13) = 0.8$ are due to the coupling between ODC solutions. Here, these two α_{ac}'s results are excluded.[31]

TABLE 3: Calculated and Corrected[a] AEs (eV) for CH_3CN and CH_3NC

		CH_3CN				CH_3NC			
method	basis set	e	a_1	e	a_1	e	e	a_1	a_1
S-KT$^{\omega B97XD}$	A	2.83	6.38	6.93	11.17	3.08	6.70	6.77	10.80
		(2.82	6.37	6.92	11.16)	(2.81	6.43	6.50	9.81)
	B	2.66	6.35	7.14	11.39	2.54	7.12	7.40	10.33
		(2.82	6.51	7.30	11.55)	(2.81	7.39	7.67	10.60)
S-KT$^{CAM\text{-}B3LYP}$	A	2.00	6.03	6.24	11.45	2.74	5.93	6.50	9.57
		(2.82	6.85	7.06	12.27)	(2.81	6.00	6.57	9.64)
	B	2.01	6.06	6.29	11.25	2.47	6.49	6.71	9.62
		(2.82	6.87	7.10	12.06)	(2.81	6.83	7.05	9.96)
S-KT$^{LC\text{-}\omega PBE}$	A	3.80	7.52	7.57	11.81	3.36	7.27	7.70	10.84
		(2.82	6.54	6.59	10.83)	(2.81	6.72	7.15	10.29)
	B	3.29	7.27	7.59	11.96	3.24	7.92	8.00	10.90
		(2.82	6.80	7.12	11.49)	(2.81	7.49	7.57	10.47)
S-KB^{PBEPBE}	A	3.94	7.43	8.19	11.89	3.95	7.83	7.84	12.24
		(2.82	6.31	7.07	10.77)	(2.81	6.69	6.70	11.10)
	B	3.72	7.82	8.58	10.89	3.53	8.21	8.77	12.17
		(2.82	6.92	7.68	9.99)	(2.81	7.49	8.05	11.45)
S-KT^{HF}	A	4.88	7.68	8.83	10.21	5.07	8.71	10.10	13.08
		(2.82	5.62	6.77	8.15)	(2.81	6.45	7.84	10.82)
	B	4.45	7.03	8.30	10.02	4.18	7.79	10.04	14.11
		(2.82	5.40	6.67	8.39)	(2.81	6.42	8.67	12.74)
KT^{PBEPBE}	A	0.12	1.69	3.60	4.02	0.89	1.86(a_1)	3.25	3.52(e)
		(2.82	4.39	6.30	6.72)	(2.81	3.78	5.17	5.43)
	B	−0.56(a_1)	−0.25(e)	0.77(a_1)	0.99(e)	−0.53	−0.47(a_1)	0.74	1.03(e)
		(2.82	3.12	4.15	4.36)	(2.81	2.87	4.08	4.37)
KT^{B3LYP}	A	0.99	2.27	4.36	5.01	0.99	2.47(a_1)	4.29	4.29(e)
		(2.82	4.10	6.18	6.83)	(2.81	4.29	6.11	6.11)
	B	−0.26(a_1)	0.58(e)	0.95(a_1)	1.24(e)	−0.15(a_1)	0.17	1.00	1.37(e)
		(2.82	3.66	4.03	4.32)	(2.81	3.13	3.96	4.33)
expt[b]		2.82	5.7	6.8	*c*	2.81	5.5	6.7	*c*

[a] The corrected values (shown in parentheses) are obtained by shifting the amount needed to bring the calculated AEs into agreement with experimental values for the LUMOs. [b] The experimental AEs are taken from ref 24a. [c] The energy value is outside the observed range.

Thus, the obtained energies of the 16a′, 17a′, 18a′, 19a′, and 20a′ orbitals are 1.32, 3.03, 3.96, 8.17, and 11.33 eV, respectively.

Next, for the a″ virtual orbitals of CH_3NCS as shown in Figure 5b, the obtained energy of the 5a″ orbital is 1.81 eV at $\alpha_{ac}(1,2) = 0.6$. The obtained energies of the 6a″ orbital are 6.25 eV at $\alpha_{ac}(2,3) = 2.5$, 6.22 eV at $\alpha_{ac}(3,4) = 1.8$, and 6.32 eV at $\alpha_{ac}(4,5) = 1.0$. Thus, the energies of the 5a″ and 6a″ orbitals are 1.81 and 6.22 eV, respectively. For the a′ virtual orbitals, the obtained energy of the 16a′ is 1.33 eV at $\alpha_{ac}(1,2) = 0.8$. The obtained energies of 17a′ orbital are 4.17 eV at $\alpha_{ac}(5,6) = 1.4$, 5.08 eV at $\alpha_{ac}(8,9) = 0.9$, and 5.12 eV at $\alpha_{ac}(9,10) = 0.8$. The obtained energies of the 18a′ are 6.59 eV at $\alpha_{ac}(7,8) = 2.2$, 6.61 eV at $\alpha_{ac}(8,9) = 1.9$, 6.77 eV at $\alpha_{ac}(9,10) = 1.4$, 6.52 eV at $\alpha_{ac}(10,11) = 1.0$, and 6.38 eV at $\alpha_{ac}(11,12) = 0.8$. The obtained energies of the 19a′ orbital are 8.63 eV at $\alpha_{ac}(11,12) = 1.4$, 7.58 eV at $\alpha_{ac}(13,14) = 0.8$, and 7.84 eV at $\alpha_{ac}(15,16) = 0.6$. The obtained energies of 20a′ orbital are 11.26 eV at $\alpha_{ac}(16,17) = 0.9$ and 10.19 eV at $\alpha_{ac}(17,18) = 0.4$. Thus, the energies of the 16a′, 17a′, 18a′, 19a′, and 20a′ orbitals are 1.33, 4.79, 6.57, 8.02, and 10.73 eV, respectively. It should be mentioned that some of the derived AEs vary by more than 1 eV. These variations may indicate that the resonance states have significant widths and may not be observed by ETS. It is particularly difficult to obtain unique energies from stabilization calculations on resonance states with significant widths.

According to our analysis of the nature of orbitals for CH_3SCN, the LUMO (16a′) essentially results from the antibonding interaction between SCN a′($\pi_{||-}$) and CH_3 4a′ σ orbitals. Orbital 17a′ is mainly from SCN 14a′(σ^*). Orbital 18a′ is mainly from SCN 13a′($\pi^*_{||}$). Orbital 19a′ is mainly from the mixing of CH_3 pseudo-$\pi^*_{||}$ with SCN 13a′ ($\pi^*_{||}$). Orbital 20a′ is essentially CH_3 6a′(σ^*). Orbital 5a″ corresponds to π-bonding interaction between SCN 4a″($\pi^*_{\perp}$) and CH_3 pseudo-$\pi^*_{\perp}$. The 6a″ orbital corresponds to π-antibonding interaction between CH_3 pseudo-$\pi^*_{\perp}$ and SCN 4a″($\pi^*_{\perp}$) orbitals. As for CH_3NCS, the 16a′ orbital is essentially derived from the NCS a′($\pi^*_{||}$). The 17a′ mainly results from the antibonding interaction between NCS a′($\pi_{||-}$) and CH_3 4a′ σ orbitals. The 18a′ orbital is mainly from the mixing of NCS 14a′(σ^*) with CH_3 pseudo-$\pi^*_{||}$. Orbital 19a′ results from the mixing of CH_3 pseudo-$\pi^*_{||}$ with NCS 13a′($\pi^*_{||}$) and 14a′(σ^*). The 20a′ orbital is mainly from CH_3 6a′ σ^*. MO 5a″ corresponds to the π-bonding interaction between CH_3 pseudo-$\pi^*_{\perp}$ and NCS a″($\pi^*_{\perp}$) orbitals. The 6a″ orbital corresponds to the π-antibonding interaction between CH_3 pseudo-$\pi^*_{\perp}$ and NCS a″($\pi^*_{\perp}$) orbitals.

The calculated AEs of CH_3SCN and CH_3NCS using the representative basis set A are summarized in Table 4. The increasing order of AEs of unfilled orbitals are 16a′ < 5a″ < 17a′ < 18a′ < 6a″ < 19a′ < 20a′ for CH_3SCN and 16a′ < 5a″ < 17a′ < 6a″ < 18a′ < 19a′ < 20a′ for CH_3NCS. According to our stabilization calculations for CH_3SCN, the 0.87 eV feature in the ET spectrum is ascribed to electron capture into the empty 16a′ orbital. The resonance at 2.37 eV can be associated with the electron capture into the 5a″ and 17a′ orbitals. The broad resonance at 3.6 eV in the ET spectrum can be ascribed to electron capture into the empty 18a′ and 6a″ orbitals. As for CH_3NCS, the electron capture into the 16a′ orbital corresponds to the resonance at 0.81 eV. The 1.83 eV feature is ascribed to the electron capture into the 5a″ orbital. The capture into the 17a′, 6a″, and 18a′ orbitals can be associated with the broad resonance at 4.0 eV. Notice that our assignments of the 3.6 eV feature for CH_3SCN and 4.0 eV feature for CH_3NCS differ from

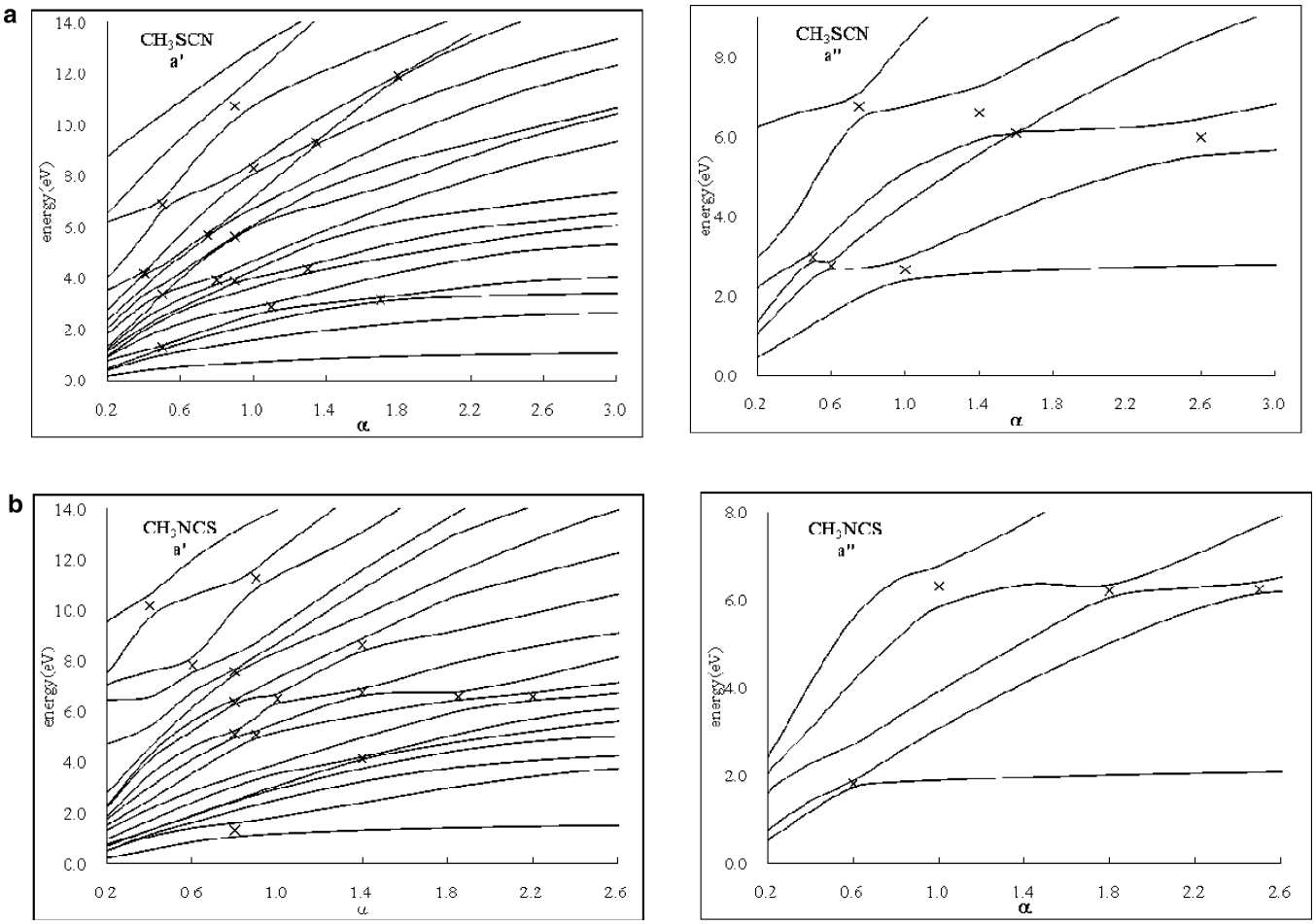

Figure 5. Stabilization graphs for CH_3SCN and CH_3NCS via the S-KT$^{\omega B97XD}$ method. Energies of a′ and a″ virtual orbitals of (a) CH_3SCN and (b) CH_3NCS as a function of α. The location of α_{ac} is marked with x.

TABLE 4: Calculated and Corrected[a] AEs (eV) for CH_3SCN and CH_3NCS

method		S-KT$^{\omega B97XD}$	S-KT$^{CAM\text{-}B3LYP}$	S-KT$^{LC\text{-}\omega PBE}$	S-KB^{PBEPBE}	S-KT^{HF}	expt[b]
CH_3SCN	16 a′	1.32 (0.87)	0.34 (0.87)	1.95 (0.87)	1.62 (0.87)	3.30 (0.87)	0.87
	5 a″	2.70 (2.03)	2.00 (2.53)	3.20 (2.49)	3.25 (2.50)	4.77 (2.34)	2.37
	17 a′	3.03 (2.58)	2.16 (2.69)	3.61 (2.90)	3.70 (2.95)	6.29 (3.86)	2.37
	18 a′	3.96 (3.51)	3.38 (3.91)	4.36 (3.65)	4.62 (3.87)	7.92 (5.49)	3.6
	6 a″	6.37 (5.70)	5.52 (6.05)	6.78 (6.07)	6.79 (6.04)	8.36 (5.93)	3.6
	19 a′	8.17 (7.72)	6.86 (7.39)	8.20 (7.49)	7.33 (6.58)	10.32 (7.89)	*c*
	20 a′	11.33 (10.88)	8.67 (9.20)	9.90 (9.19)	10.73 (9.98)	12.62 (10.19)	*c*
CH_3NCS	16 a′	1.33 (0.81)	0.79 (0.81)	1.76 (0.81)	2.00 (0.81)	3.56 (0.81)	0.81
	5 a″	1.81 (1.29)	1.28 (1.36)	2.82 (1.94)	2.71 (1.52)	3.94 (1.19)	1.83
	17 a′	4.79 (4.27)	3.41 (3.43)	5.44 (4.56)	5.00 (4.11)	6.86 (4.11)	4.0
	6 a″	6.22 (5.70)	5.58 (5.66)	6.79 (5.91)	6.94 (5.61)	8.37 (5.62)	4.0
	18 a′	6.57 (6.05)	5.66 (5.74)	7.01 (6.13)	6.95 (5.62)	8.53 (5.78)	4.0
	19 a′	8.02 (7.50)	7.41 (7.49)	8.95 (8.07)	8.16 (6.83)	10.94 (8.19)	*c*
	20 a′	10.73 (10.21)	9.77 (9.85)	11.79 (10.91)	10.88 (9.55)	12.63 (9.88)	*c*

[a] The corrected values (shown in parentheses) are obtained by shifting the amount needed to bring the calculated AEs into agreement with experimental values for the LUMOs. [b] The AEs are taken from ref 24a. [c] The energy value is outside the observed range.

those of the previous studies that were attributed to the σ^*_{CS} resonances.[24a] Their spectral interpretation was partially supported by conventional calculations. However, the temporary anions cannot be handled straightforwardly by conventional methods without special techniques such as a stabilization method being utilized.[17a] Our corrected AEs are in agreement with the experimental data, and the ordering of unfilled orbitals is consistent for all the AC density functional. Hence, the assignment of the spectrum should be plausible.

4. Conclusion

The energies of filled and unfilled orbitals in CH_3CN, CH_3NC, CH_3SCN, and CH_3NCS have been systematically studied. The obtained results have demonstrated that the KT using long-range correction functional and KB method using local functional can yield improvement in values of IPs. In addition, the stabilization method can yield better energy results of temporary anion states than other methods without stabilization. Furthermore, our

calculations have indicated the presence of several σ^* and π^* temporary anion states on these molecules. It is believed that AC density functionals can be very useful in the studies of temporary anion states for pseudohalides.

Acknowledgment. We thank the reviewers for valuable comments during the revision process and National Center for High-Performance Computing for the computational resources provided. This work was supported by National Science Council of Republic of China under grant number NSC 99-2113-M029-003.

References and Notes

(1) (a) Heintz, R. A.; Zhao, H.; Ouyang, X.; Grandinetti, G.; Cowen, J.; Dunbar, K. R. *Inorg. Chem.* **1999**, *38*, 144. (b) Kivala, M.; Diederich, F. *Acc. Chem. Res.* **2009**, *42*, 235.

(2) Mukerjee, A. K.; Ashare, R. *Chem. Rev.* **1991**, *91*, 1.

(3) (a) Heimer, T. A.; Bignozzi, C. A.; Meyer, G. J. *J. Phys. Chem.* **1993**, *97*, 11987. (b) Nazeeruddin, M. K.; Kay, A.; Rodicio, I.; Humphry-Baker, R.; Muller, E.; Liska, P.; Vlachopoulos, N.; Grätzel, M. *J. Am. Chem. Soc.* **1993**, *115*, 6382. (c) Hagfeldt, M.; Grätzel, M. *Acc. Chem. Res.* **2000**, *33*, 269.

(4) Dömling, A. *Chem. Rev.* **2006**, *106* (1), 17.

(5) Aune, T. M.; Thomas, E. L. *Biochemistry* **1978**, *17*, 1005.

(6) Sharma, A. K.; Sharma, A.; Desai, D.; Madhunapantula, S. V.; Huh, S. J.; Robertson, G. P.; Amin, S. *J. Med. Chem.* **2008**, *51* (24), 7820.

(7) Rabalais, J. W. *Principles of Ultraviolet Photoelectron Spectroscopy*; John Wiley and Sons: New York, 1977.

(8) Sanche, L.; Schulz, G. J. *Phys. Rev. A* **1972**, *5*, 1672.

(9) Jordan, K. D.; Burrow, P. D. *Chem. Rev.* **1987**, *87*, 557.

(10) Koopmans, T. *Physica* **1934**, *1*, 104.

(11) (a) Falcetta, M. F.; Jordan, K. D. *J. Phys. Chem.* **1990**, *94*, 5666. (b) Falcetta, M. F.; Jordan, K. D. *J. Am. Chem. Soc.* **1991**, *113*, 2903. (c) Falcetta, M. F.; Jordan, K. D. *Chem. Phys. Lett.* **1999**, *300*, 588.

(12) Burrow, P. D.; Howard, A. E.; Johnston, A. R.; Jordan, K. D. *J. Phys. Chem.* **1992**, *96*, 7570.

(13) (a) Juang, C.-Y.; Chao, J. S.-Y. *J. Phys. Chem.* **1994**, *98*, 13506. (b) Chen, C.-S.; Feng, T.-H.; Chao, J. S.-Y. *J. Phys. Chem.* **1995**, *99*, 8629. (c) Wei, Y.-H.; Cheng, H.-Y. *J. Phys. Chem. A* **1998**, *102*, 3560.

(14) Kohn, W.; Sham, L. J. *Phys. Rev. A* **1965**, *140*, 1133.

(15) (a) Perdew, J. P.; Levy, M. *Phys. Rev. Lett.* **1983**, *51*, 1884. (b) Baerends, E. J.; Gritsenko, O. V. *J. Phys. Chem.* **1997**, *101*, 5383. (c) Baerends, E. J. *Theor. Chem. Acc.* **2000**, *103*, 265. (d) Chong, D. P.; Gritsenko, O. V.; Baerends, E. J. *J. Chem. Phys.* **2002**, *116*, 1760. (d) Gritsenko, O. V.; Baerends, E. J. *J. Chem. Phys.* **2002**, *117*, 9154.

(16) Salzner, U.; Baer, R. *J. Chem. Phys.* **2009**, *131*, 231101.

(17) (a) Simons, J. *J. Phys. Chem. A* **2008**, *112*, 6401. (b) Rienstra-Kiracofe, J. C.; Tschumper, G. S.; Schaefer, H. F., III; Nandi, S.; Ellison, G. B. *Chem. Rev.* **2002**, *102*, 231.

(18) (a) Tozer, D. J.; De Proft, F. *J. Phys. Chem. A* **2005**, *109*, 8923. (b) Tozer, D. J.; De Proft, F. *J. Chem. Phys.* **2007**, *127*, 034108. (c) De Proft, F.; Sablon, N.; Tozer, D. J.; Geerlings, P. *Faraday Discuss.* **2007**, *135*, 151. (d) Sablon, N.; De Proft, F.; Geerlingsa, P.; Tozer, D. J. *Phys. Chem. Chem. Phys.* **2007**, *9*, 5880. (e) Teale, A. M.; De Proft, F.; Tozer, D. J. *J. Chem. Phys.* **2008**, *129*, 044110. (f) Hajgató, B.; Deleuze, M. S.; Tozer, D. J.; De Proft, F. *J. Chem. Phys.* **2008**, *129*, 084308.

(19) Chai, J.-D.; Head-Gordon, M. *Phys. Chem. Chem. Phys.* **2008**, *10*, 6615.

(20) Yanai, T.; Tew, D. P.; Handy, N. C. *Chem. Phys. Lett.* **2004**, *393*, 51.

(21) Vydrov, O. A.; Scuseria, G. E.; Perdew, J. P. *J. Chem. Phys.* **2007**, *126*, 154109.

(22) (a) Hazi, A. U.; Taylor, H. S. *Phys. Rev. A* **1970**, *1*, 1109. (b) Taylor, H. S. *Adv. Chem. Phys.* **1970**, *18*, 91. (c) Fels, M. F.; Hazi, A. U. *Phys. Rev. A* **1972**, *5*, 1236. (d) Taylor, H. S.; Hazi, A. U. *Phys. Rev. A* **1976**, *14*, 2071.

(23) (a) Cheng, H.-Y.; Shih, C.-C. *J. Phys. Chem. A* **2009**, *113*, 1548. (b) Cheng, H.-Y.; Shih, C.-C.; Chang, J.-T. *J. Phys. Chem. A* **2009**, *113*, 9551. (c) Cheng, H.-Y.; Chang, J.-T.; Shih, C.-C. *J. Phys. Chem. A* **2010**, *113*, 2920.

(24) (a) Hitchcock, A. P.; Tronc, M.; Modelli, A. *J. Phys. Chem.* **1989**, *93*, 3068. (b) Edard, F.; Hitchcock, A. P.; Tronc, M. *J. Phys. Chem.* **1990**, *94*, 2768.

(25) (a) Frey, R. F.; Simons, J. *J. Chem. Phys.* **1986**, *84*, 4462. (b) Thompson, T. C.; Truhlar, D. G. *Chem. Phys. Lett.* **1982**, *92*, 71. (c) Chao, J. S.-Y.; Falcetta, M. F.; Jordan, K. D. *J. Chem. Phys.* **1990**, *93*, 1125. (d) Chao, J. S.-Y. *Chem. Phys. Lett.* **1991**, *179*, 169.

(26) Mandelshtam, V. A.; Ravuri, T. R.; Taylor, H. S. *Phys. Rev. Lett.* **1993**, *70*, 1932.

(27) Falcatta, M. F.; Chui, Y.; Jordan, K. D. *J. Phys. Chem.* **2000**, *1044*, 9605.

(28) (a) The midpoint method (ref 12) is applicable when its results were compared with those obtained from the more rigorous analytic continuation method (ref 19 in ref 13a). (b) The energy of the temporary anion state can also be estimated from the avoided crossings between the eigenvalues of the stabilization graphs (Simons, J. *J. Chem. Phys.* **1981**, *75*, 2465.) or the inspection of the stabilization graph (ref 27).

(29) Perdew, J. P.; Burke, K.; Ernzerhof, M. *Phys. Rev. Lett.* **1996**, *77*, 3865.

(30) Frisch, M. J.; Trucks, G. W.; Schlegel, H. B.; Scuseria, G. E.; Robb, M. A.; Cheeseman, J. R.; Scalmani, G.; Barone, V.; Mennucci, B.; Petersson, G. A.; Nakatsuji, H.; Caricato, M.; Li, X.; Hratchian, H. P.; Izmaylov, A. F.; Bloino, J.; Zheng, G.; Sonnenberg, J. L.; Hada, M.; Ehara, M.; Toyota, K.; Fukuda, R.; Hasegawa, J.; Ishida, M.; Nakajima, T.; Honda, Y.; Kitao, O.; Nakai, H.; Vreven, T.; Montgomery, J. A., Jr.; Peralta, J. E.; Ogliaro, F.; Bearpark, M.; Heyd, J. J.; Brothers, E.; Kudin, K. N.; Staroverov, V. N.; Kobayashi, R.; Normand, J.; Raghavachari, K.; Rendell, A.; Burant, J. C.; Iyengar, S. S.; Tomasi, J.; Cossi, M.; Rega, N.; Millam, J. M.; Klene, M.; Knox, J. E.; Cross, J. B.; Bakken, V.; Adamo, C.; Jaramillo, J.; Gomperts, R.; Stratmann, R. E.; Yazyev, O.; Austin, A. J.; Cammi, R.; Pomelli, C.; Ochterski, J. W.; Martin, R. L.; Morokuma, K.; Zakrzewski, V. G.; Voth, G. A.; Salvador, P.; Dannenberg, J. J.; Dapprich, S.; Daniels, A. D.; Farkas, O.; Foresman, J. B.; Ortiz, J. V.; Cioslowski, J.; Fox, D. J. *Gaussian 09*, Revision A.02; Gaussian, Inc.: Wallingford, CT, 2009.

(31) The ODC solutions themselves may interact with each other (refs 13b and 41 in ref 23a).

(32) Pasinszki, T.; Yamakado, H.; Ohno, K. *J. Phys. Chem.* **1995**, *99*, 14678.

(33) Pasinszki, T.; Yamakado, H.; Ohno, K. *J. Phys. Chem.* **1993**, *97*, 12718.

(34) Vydrov, O. A.; Scuseria, G. E. *J. Chem. Phys.* **2005**, *122*, 184107.

(35) Dutoi, A. D.; Head-Cordan, M. *Chem. Phys. Lett.* **2006**, *422*, 230.

JP109466J